

# Two routes to the one-dimensional discrete nonpolynomial Schrödinger equation

G. Gligorić<sup>1</sup>, A. Maluckov<sup>2</sup>, L. Salasnich<sup>3</sup>, B. A. Malomed<sup>4</sup> and Lj. Hadžievski<sup>1</sup>

<sup>1</sup> *Vinča Institute of Nuclear Sciences, P.O. Box 522, 11001 Belgrade, Serbia*

<sup>2</sup> *Faculty of Sciences and Mathematics, University of Niš, P.O. Box 224, 18001 Niš, Serbia*

<sup>3</sup> *CNR-INFM and CNISM, Department of Physics "Galileo Galilei",  
University of Padua, Via Marzolo 8, 35131 Padua, Italy*

<sup>4</sup> *Department of Physical Electronics, School of Electrical Engineering,  
Faculty of Engineering, Tel Aviv University, Tel Aviv 69978, Israel*

The Bose-Einstein condensate (BEC), confined in a combination of the cigar-shaped trap and axial optical lattice, is studied in the framework of two models described by two versions of the one-dimensional (1D) discrete nonpolynomial Schrödinger equation (NPSE). Both models are derived from the three-dimensional Gross-Pitaevskii equation (3D GPE). To produce “model 1” (which was derived in recent works), the 3D GPE is first reduced to the 1D continual NPSE, which is subsequently discretized. “Model 2”, that was not considered before, is derived by first discretizing the 3D GPE, which is followed by the reduction of the dimension. The two models seem very different; in particular, model 1 is represented by a single discrete equation for the 1D wave function, while model 2 includes an additional equation for the transverse width. Nevertheless, numerical analyses show similar behaviors of fundamental unstaggered solitons in both systems, as concerns their existence region and stability limits. Both models admit the collapse of the localized modes, reproducing the fundamental property of the self-attractive BEC confined in tight traps. Thus, we conclude that the fundamental properties of discrete solitons predicted for the strongly trapped self-attracting BEC are reliable, as the two distinct models produce them in a nearly identical form. However, a difference between the models is found too, as strongly pinned (very narrow) discrete solitons, which were previously found in model 1, are not generated by model 2 – in fact, in agreement with the continual 1D NPSE, which does not have such solutions either. In that respect, the newly derived model provides for a more accurate approximation for the trapped BEC.

PACS numbers: 03.75.Lm; 05.45.Yv

The dynamics of a dilute quantum gas which forms the Bose-Einstein condensate (BEC) is very accurately described by the three-dimensional Gross-Pitaevskii equation (3D GPE). This equation treats effects of collisions between atoms in the condensate in the mean-field approximation. In experimentally relevant settings, the BEC is always confined by a trapping potential. In many cases, the trap is designed to have the “cigar-shaped” form, allowing an effective reduction of the dimension from 3 to 1. In turn, the 1D dynamics of the trapped condensate may be controlled by means of an additional periodic potential, induced by an optical lattice (OL), which acts along the axis of the “cigar”. If the OL potential is sufficiently strong, the eventual dynamical model reduces to a 1D discrete equation. In both the continual and discrete versions of the 1D description, a crucially important feature is the form of the nonlinearity in the respective equations. In the limit of low density, the nonlinearity is cubic – the same as in the underlying 3D GPE. In the general case, a consistent derivation, which starts from the cubic nonlinearity in 3D, leads to 1D equations with a nonpolynomial nonlinearity, the respective model being called the “nonpolynomial Schrödinger equation” (NPSE). The discrete limit of the latter equation, corresponding to the action of the strong axial OL potential, was derived and investigated recently. An essential asset of both versions of the NPSE, continual and discrete ones, is that they predict the onset of the collapse (formation of a singularity in the condensate with attraction between atoms) in the framework of the 1D description, thus complying with the fundamental property of the BEC which was predicted by the underlying 3D GPE and observed experimentally. However, in the case when the OL potential is very strong, an alternative way to derive the 1D discrete model may start with the discretization of the 3D GPE, followed by the reduction of the dimension in the cigar-shaped trap. In this work, we report a new discrete model (“model 2”) derived in this way, which seems very different from the previously known discrete 1D NPSE (which we call “model 1”). In particular, while model 1 amounts to a single discrete equation for the 1D complex wave function, model 2 incorporates an additional equation for the transverse width. Nevertheless, numerical analysis performed in the present work shows remarkably similar behavior of fundamental localized modes, in the form of unstaggered discrete solitons, in both systems. The similarity pertains to the existence region for the solitons and their stability limits. Importantly, both models admit the collapse, and produce similar predictions for the collapse threshold. Thus, basic properties of discrete solitons found in the model of the strongly trapped BEC are trustworthy,

as they are reproduced independently by the two very different models. Nevertheless, a difference between the two models is also found: very narrow discrete solitons, which exist in model 1, are absent in model 2. In fact, the continual 1D NPSE does not give rise to such extremely narrow solutions either, thus indicating that the newly derived model, although having a more complex mathematical form, eventually provides a more accurate approximation.

## I. INTRODUCTION

The dynamics of Bose-Einstein condensates (BECs) made of dilute ultracold gases of bosonic atoms obeys the 3D Gross-Pitaevskii equation (GPE) in the mean-field approximation [1]. An effective 1D equation can be derived from the 3D GPE to describe the BEC dynamics in prolate ("cigar-shaped") traps [2]-[8]. In the simplest case, which corresponds to a sufficiently low BEC density, the reduced 1D equation amounts to the cubic nonlinear Schrödinger equation (NLSE) [9]. A significant restriction in the use of the 1D cubic NLSE in this context is its failure to predict the onset of the collapse of localized modes, which was theoretically predicted in 3D models and experimentally observed in the self-attractive BEC [10, 11]. This problem can be resolved by the more accurate reduction of the 3D GPE to the 1D nonlinear Schrödinger equation with a *nonpolynomial* nonlinearity (NPSE) [4], [5], without imposing the constraint of a very low density. The 1D NPSE model with self-attractive nonlinearity enables the description of the collapse dynamics, and yields results which are accurately reproduced by direct simulations of the underlying 3D GPE [12]. An intermediate approximation, which can be obtained from the expansion of the NPSE, is represented by the 1D NLSE with the self-focusing cubic and quintic terms. This approximation may be sufficient for some particular purposes [3, 6, 7].

On the other hand, the BEC trapped in a very deep optical lattice (OL) can be well described by the corresponding discrete equations. In particular, discrete forms of the 1D GPE with the cubic nonlinearity [13, 14, 15] and 1D NPSE [16, 17] have been studied in detail. Basic features of the 1D continual models describing the BEC trapped in a deep OL find their counterparts in the discrete models, a significant one being the ability of the discrete 1D NPSE to describe the onset of the collapse predicted by the corresponding continual equation [16, 17].

Thus, the previously explored 1D discrete BEC models relied upon the discretization after the reduction of the dimension from 3 to 1 within the framework of the continual equations. However, an alternative approach is possible too, in the situation when the OL is stronger than the cigar-shaped potential: one should first discretize the 3D GPE in the axial direction, and then reduce the dimension to 1 [5], opposite to the previously developed derivation [4]. The purpose of the present work is to derive the discrete model in this way, which, to the best of our knowledge, has not been done before. Naturally, the two different routes lead to quite different discrete systems. In particular, the one derived in this work involves two sets of discrete variables (the wave function and transverse width), rather than the single set on which previously studied models were based. Our purpose is not only to derive the alternative system, but also to study generic properties of fundamental unstaggered solitons in it, and compare the results with those obtained in the earlier known discrete NPSE. In fact, we will conclude that, despite a very different form of the new model, it gives rise to results quite similar to those produced by the discrete NPSE. Thus, despite significant differences in the form of the "competing" models, the physical predictions for the discrete BEC solitons are essentially the same, which attests to the reliability of these results.

The paper is structured as follows. The new model is derived in section 2. Basic results for the existence, stability and dynamical behavior of fundamental discrete solitons in it are reported and compared to their counterparts predicted by the usual 1D discrete NPSE in section 3. The paper is concluded by section 4.

## II. THE DERIVATION OF THE DISCRETE ONE-DIMENSIONAL SYSTEMS

The starting point of the consideration is the 3D GPE, which governs the evolution of macroscopic wave function  $\psi(\mathbf{r}, t)$  of the dilute BEC near zero temperature [1]. This equation can be derived from the following action functional [4],

$$S = \int dt d\mathbf{r} \psi^*(\mathbf{r}, t) \left( i\hbar \frac{\partial}{\partial t} + \frac{\hbar^2}{2m} (\nabla_{\perp}^2 + \frac{\partial^2}{\partial z^2}) - V_0 \cos(2kz) - \frac{m\omega_{\perp}^2}{2} (x^2 + y^2) - \frac{1}{2} \gamma (N-1) |\psi|^2 \right) \psi(\mathbf{r}, t), \quad (1)$$

where  $\gamma = 4\pi\hbar^2 a_s/m$  is the strength of the interaction between bosons,  $a_s$  the  $s$ -wave scattering length,  $N$  the number of bosonic atoms,  $m$  the atomic mass, and  $\omega_{\perp}$  the frequency of the transverse harmonic confinement. The

corresponding 3D GPE is written as

$$i\hbar\frac{\partial}{\partial t}\psi = \left[ -\frac{\hbar^2}{2m}\nabla^2 + V_0 \cos(2kz) + \frac{m\omega_\perp^2}{2}(x^2 + y^2) + \gamma(N-1)|\psi|^2 \right] \psi. \quad (2)$$

Expressing the length in units of  $a_\perp$ , time in units of  $\omega_\perp^{-1}$  and energy in units of  $\hbar\omega_\perp$ , the 3D GPE is cast in the scaled form,

$$i\frac{\partial}{\partial t}\psi = \left[ -\frac{1}{2}(\nabla_\perp^2 + \frac{\partial^2}{\partial z^2}) + V_0 \cos(2kz) + \frac{1}{2}(x^2 + y^2) + 2\pi\Gamma|\psi|^2 \right] \psi, \quad (3)$$

where  $\Gamma = 2(N-1)a_s/a_\perp$  is the effective strength of the self-interaction, and  $a_\perp = \sqrt{\hbar/(m\omega_\perp)}$  is the characteristic length of the transverse confinement. Notice that  $a_s < 0$ , i.e.,  $\Gamma < 0$  in Eq. (3), corresponds to the attraction between bosons.

Below, we consider the derivation of two alternative forms of the 1D discrete approximation. The previously known ‘‘model 1’’ is derived starting with reduction of the 3D GPE to the 1D NPSE, which is then discretized [16, 17]. Here, we briefly recapitulate this route of the derivation, for the purpose of the comparison with novel ‘‘model 2’’, which is obtained from the 3D GPE by *first* discretizing it, and *then* reducing the resulting system to the 1D form.

### A. Model 1: the reduction of the dimension followed by the discretization

The derivation of model 1 starts with the dimensional reduction, which is performed by the minimization of action functional (1), choosing the wave function in the form of

$$\psi(\mathbf{r}, t) = \frac{\exp[-(x^2 + y^2)/(2\sigma^2(z, t))]}{\sqrt{\pi}\sigma(z, t)} f(z, t), \quad (4)$$

where real  $\sigma$  is the local width of the transverse confinement, and complex 1D (axial) wave function  $f$  is normalized,

$$\int_{-\infty}^{+\infty} |f(z)|^2 dz = 1 \quad (5)$$

[4]. Inserting trial wave function (4) in Eq. (1) and performing the integration over  $x$  and  $y$ , the action can be written as

$$S = \int dt \int_{-\infty}^{+\infty} dz f^* \left( i\frac{\partial}{\partial t} + \frac{1}{2}\frac{\partial^2}{\partial z^2} - V_0 \cos(2qz) + \frac{\Gamma}{\sigma^2}|\psi|^2 - \frac{1}{2}\left(\frac{1}{\sigma^2} + \sigma^2\right) \right) f, \quad (6)$$

in the approximation which neglects  $\partial\sigma/\partial z$  [4]. The Euler-Lagrange equations derived from Eq. (6) by varying with respect to  $f^*$  and  $\sigma$ ,

$$i\frac{\partial f}{\partial t} = \left[ -\frac{1}{2}\frac{\partial^2}{\partial z^2} + V_0 \cos(2qz) + \frac{\Gamma}{\sigma^2}|f|^2 + \frac{1}{2}\left(\frac{1}{\sigma^2} + \sigma^2\right) \right] f, \quad (7)$$

$$\sigma^4 = 1 + \Gamma|f|^2, \quad (8)$$

may be combined into the equation (NPSE) derived in Ref. [4], namely,

$$i\frac{\partial f}{\partial t} = \left[ -\frac{1}{2}\frac{\partial^2}{\partial z^2} + V_0 \cos(2qz) + \frac{1 + (3/2)\Gamma|f|^2}{\sqrt{1 + \Gamma|f|^2}} \right] f. \quad (9)$$

Assuming that OL potential in this equation is strong enough, one can further derive the discrete version of the 1D NPSE [16, 17]. To this end, the continual wave function is approximated by a superposition of orthonormal modes  $W_n$  (such as Wannier functions), which are tightly confined in a vicinity of local potential minima,  $z_n = \pi n/q$ , with integer  $n$ :

$$f(z, t) = \sum_n f_n(t)W_n(z), \quad (10)$$

$f_n$  being the respective complex amplitudes. This decomposition is made unique by imposing a condition that the largest value of each local function  $W_n$  is 1 [16]. Next, one may insert this ansatz in Eq. (7), multiply the resulting equation by the complex conjugate of the local mode, and integrate over  $z$ . The so derived 1D discrete NPSE, together with the discrete version of equation (8), take the form of

$$i\frac{\partial}{\partial t}f_n = \left[ \frac{1}{2} \left( \frac{1}{\sigma_n^2} + \sigma_n^2 \right) + \epsilon \right] f_n - C(f_{n+1} + f_{n-1}) + \frac{g}{\sigma_n^2}|f_n|^2 f_n, \quad (11)$$

$$\sigma_n^4 = 1 + g|f_n|^2, \quad (12)$$

where the local norms and parameters  $\epsilon$ ,  $C$  and  $g$  are

$$\begin{aligned} \epsilon &\equiv \int W_n^*(z) \left[ -\frac{1}{2} \frac{\partial^2}{\partial z^2} + V_0 \cos(2kz) \right] W_n(z) dz, \\ C &\equiv - \int W_{n+1}^*(z) \left[ -\frac{1}{2} \frac{\partial^2}{\partial z^2} + V_0 \cos(2kz) \right] W_n(z) dz, \\ g &\equiv \Gamma \int |W_n(z)|^4 dz. \end{aligned} \quad (13)$$

In the tight-binding approximation,  $C$  is positive definite.

In what follows below, the discrete system based on Eqs. (11) and (12) is referred to as ‘‘model 1’’. These equations correspond to the Lagrangian,

$$L_{\text{eff}} = \sum_n \left\{ f_n^* \left[ i\frac{\partial}{\partial t} - \frac{1}{2} \left( \frac{1}{\sigma_n^2} + \sigma_n^2 \right) - \epsilon \right] f_n + C f_n^* (f_{n+1} + f_{n-1}) - \frac{g}{2\sigma_n^2} |f_n|^4 \right\}. \quad (14)$$

Model 1 conserves two dynamical invariants, *viz.*, the norm (alias ‘‘power’’) and Hamiltonian,

$$\mathcal{N} = \sum_n |f_n|^2, \quad \mathcal{H} = \sum_n \left( C|f_n - f_{n+1}|^2 + \sqrt{1 - g|f_n|^2} |f_n|^2 \right). \quad (15)$$

## B. Model 2: the discretization followed by the reduction of the dimension

The derivation of the novel system starts with the direct discretization of the 3D GPE, i.e., Eq. (2), by adopting the following ansatz for the wave function,

$$\psi(x, y, z, t) = \sum_n \phi_n(x, y) W_n(z), \quad (16)$$

where  $W_n(z)$  is the same set of local modes as in Eq. (10). We insert this ansatz in Eq. (2), multiply the resulting equation by  $W_n^*$ , and integrate the result over  $z$ . This leads to the semi-discrete equation,

$$i\frac{\partial}{\partial t}\phi_n = \left[ -\frac{1}{2}\nabla_{\perp}^2 + \frac{1}{2}(x^2 + y^2) + \epsilon \right] \phi_n - C(\phi_{n+1} + \phi_{n-1}) + 2\pi g|\phi_n|^2 \phi_n, \quad (17)$$

where  $\nabla_{\perp}^2$  acts on coordinates  $x$  and  $y$ , and parameters  $\epsilon$ ,  $C$  and  $g$  are defined as per Eqs. (13).

Equation (17) can be derived from the corresponding Lagrangian,

$$L = \int_{-\infty}^{+\infty} dx \int_{-\infty}^{+\infty} dy \sum_n \left[ \phi_n^* \left[ i\frac{\partial}{\partial t} + \frac{1}{2}\nabla_{\perp}^2 - \frac{1}{2}(x^2 + y^2) - \epsilon \right] \phi_n + C\phi_n^*(\phi_{n+1} + \phi_{n-1}) - \pi g|\phi_n|^4 \right]. \quad (18)$$

The further simplification is performed by substituting ansatz

$$\phi_n(x, y, t) = \frac{1}{\sqrt{\pi}\sigma_n(t)} \exp\left(-\frac{x^2 + y^2}{2\sigma_n^2(t)}\right) f_n(t) \quad (19)$$

into Lagrangian (18) and integrating over the  $(x, y)$  plane, which eventually leads to an effective Lagrangian for 1D discrete fields  $f_n(t)$  and  $\sigma_n(t)$ ,

$$\begin{aligned} L &= \sum_n \left\{ f_n^* \left[ i\frac{\partial}{\partial t} - \frac{1}{2} \left( \frac{1}{\sigma_n^2} + \sigma_n^2 \right) - \epsilon \right] f_n \right. \\ &\quad \left. + 2C \frac{\sigma_n \sigma_{n+1}}{\sigma_n^2 + \sigma_{n+1}^2} (f_n^* f_{n+1} + f_{n-1}^* f_n) - \frac{g}{2\sigma_n^2} |f_n|^4 \right\}. \end{aligned} \quad (20)$$

The Euler-Lagrange equations derived from Eq. (20) by varying the Lagrangian with respect to  $f_n^*$  and  $\sigma_n$  are

$$i \frac{\partial}{\partial t} f_n = \left[ \frac{1}{2} \left( \frac{1}{\sigma_n^2} + \sigma_n^2 \right) + \epsilon \right] f_n + \frac{g}{\sigma_n^2} |f_n|^2 f_n - C \left( \frac{2\sigma_n \sigma_{n+1}}{\sigma_n^2 + \sigma_{n+1}^2} f_{n+1} + \frac{2\sigma_n \sigma_{n-1}}{\sigma_n^2 + \sigma_{n-1}^2} f_{n-1} \right), \quad (21)$$

$$\begin{aligned} |f_n|^2 \frac{1 + g|f_n|^2 - \sigma_n^4}{\sigma_n^3} + 2C(f_{n+1}^* f_n + f_{n+1} f_n^*) \frac{\sigma_{n+1}(\sigma_{n+1}^2 - \sigma_n^2)}{(\sigma_{n+1}^2 + \sigma_n^2)^2} \\ + 2C(f_{n-1}^* f_n + f_{n-1} f_n^*) \frac{\sigma_{n-1}(\sigma_{n-1}^2 - \sigma_n^2)}{(\sigma_{n-1}^2 + \sigma_n^2)^2} = 0. \end{aligned} \quad (22)$$

Equations (21) and (22) conserve the respective norm and Hamiltonian, which are [cf. Eq. (15)]

$$\begin{aligned} \mathcal{N} &= \sum_n |f_n|^2, \\ \mathcal{H} &= \sum_n \left\{ f_n^* \left[ \frac{1}{2} \left( \frac{1}{\sigma_n^2} + \sigma_n^2 \right) + \epsilon \right] f_n - 2C \frac{\sigma_n \sigma_{n+1}}{\sigma_n^2 + \sigma_{n+1}^2} (f_n^* f_{n+1} + f_{n-1}^* f_n) + \frac{g}{2\sigma_n^2} |f_n|^4 \right\}. \end{aligned} \quad (23)$$

It is worthy to note that Eq. (12) in model 1 involves only  $\sigma_n$  (without coupling to  $\sigma_{n\pm 1}$ ), because the corresponding spatial derivative,  $\partial\sigma/\partial z$ , was neglected in the underlying expression (6). On the contrary to that, Eq. (22) in model 2 couples  $\sigma_n$  to  $\sigma_{n\pm 1}$ , as this coupling is implicitly retained by expressions (18) and (19). For that reason,  $\sigma_n^2$  cannot be explicitly found from Eq. (22), hence model 2, unlike model 1, cannot be reduced to a single equation for the discrete wave function. Nevertheless, model 2 is amenable to a consistent numerical analysis, see below. The two models can be made formally equivalent only if transverse widths  $\sigma_n$  are postulated to be constant ( $t$ - and  $n$ -independent), in which case either system reduces to the standard discrete 1D NLSE. Finally, it is worthy to mention that both models, i.e., Eqs. (11), (12), on the one side and Eq. (21) on the other, take identical limit forms in the anticontinuum limit,  $C = 0$ .

### III. FUNDAMENTAL BRIGHT SOLITONS

#### A. The existence of fundamental solitons

In this section we present families of fundamental bright-soliton solutions to Eqs. (21) and (22), identify their stability and compare them to the corresponding soliton families in model 1 [16, 17]. If the nonlinearity is attractive ( $g < 0$ ), the stationary solutions of models 1 and 2 with chemical potential  $\mu$  are sought for by the substitution into Eqs. (11), (12) and (21), respectively, of

$$f_n(t) = |g|^{-1/2} u_n \exp(-i\mu t). \quad (24)$$

In doing so, we assume that  $\epsilon = 2C$  was fixed by means of an obvious additional shift of the chemical potential. Then, real discrete functions  $u_n$  obey stationary equations, which are

$$\mu u_n = -C(u_{n+1} + u_{n-1} - 2u_n) + \frac{1 - (3/2)u_n^2}{\sqrt{1 - u_n^2}} u_n \quad (25)$$

in model 1, and

$$\begin{aligned} \mu u_n &= - \left[ \frac{1}{2} \left( \frac{1}{\sigma_n^2} + \sigma_n^2 \right) + 2C \right] u_n + \frac{g}{\sigma_n^2} |u_n|^2 u_n \\ &\quad - C \left( \frac{2\sigma_n \sigma_{n+1}}{\sigma_n^2 + \sigma_{n+1}^2} u_{n+1} + \frac{2\sigma_n \sigma_{n-1}}{\sigma_n^2 + \sigma_{n-1}^2} u_{n-1} \right) \end{aligned} \quad (26)$$

in model 2. In the latter case, widths  $\sigma_n$  are to be found from Eq. (22), which takes the form of

$$\begin{aligned} |u_n|^2 \frac{1 + g|u_n|^2 - \sigma_n^4}{\sigma_n^3} + 2C(u_{n+1}^* u_n + u_{n+1} u_n^*) \frac{\sigma_{n+1}(\sigma_{n+1}^2 - \sigma_n^2)}{(\sigma_{n+1}^2 + \sigma_n^2)^2} \\ + 2C(u_{n-1}^* u_n + u_{n-1} u_n^*) \frac{\sigma_{n-1}(\sigma_{n-1}^2 - \sigma_n^2)}{(\sigma_{n-1}^2 + \sigma_n^2)^2} = 0. \end{aligned} \quad (27)$$

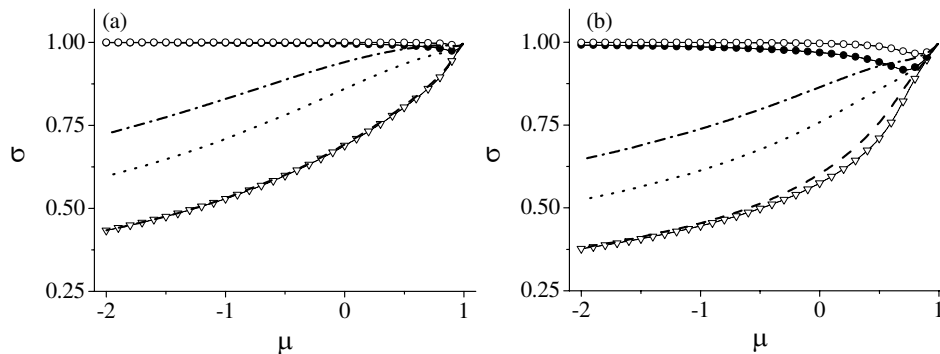


FIG. 1: Values of the transverse width,  $\sigma_n$ , as functions of the chemical potential,  $\mu$ , for fundamental on-site solitons in model 1 (the ordinary model) are shown by curves which are marked by triangles for the central site, full circles – for the first neighbors, and empty circles – for the second neighbors to the central site. In model 2 (the new system) the values of  $\sigma_n$  for fundamental on-site solitons are shown by dashed lines for the central site, dotted lines – the first neighbors, and dashed-dotted lines – the second neighbors to the central site. The inter-site coupling constant is  $C = 0.2$  (a) and  $C = 0.8$  (b).

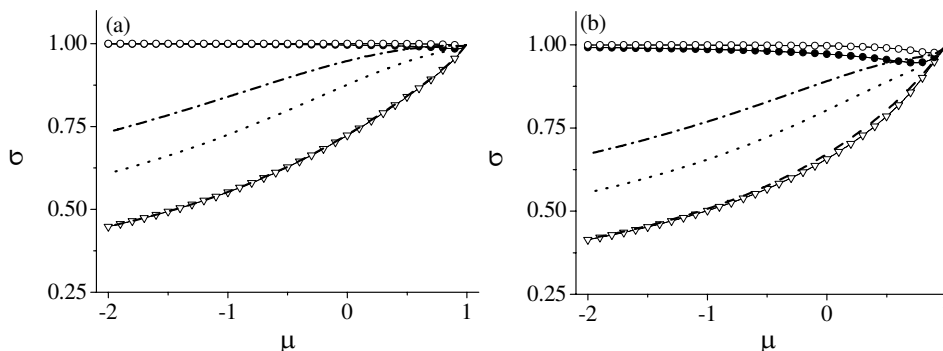


FIG. 2: The same as in Fig. 1, but for families of inter-site solitons found in both models 1 and 2.

Stationary equations (25) and (26) were solved numerically, using an algorithm based on the modified Powell minimization method [14, 16]. The initial ansatz used to construct on-site and inter-site-centered discrete solitons in model 1 was, respectively,  $\{u_n^{(0)}\} = (\dots, 0, A, 0, \dots)$  and  $(\dots, 0, A, A, 0, \dots)$ , where  $A$  is a real constant obtained from Eq. (25) in the corresponding approximation. These soliton solutions are then used as an initial ansatz to generate discrete solitons in model 2. Results reported below were obtained in the lattice composed of 101 or 100 sites, for the on-site and inter-site configurations, respectively. It was checked that the results do not alter if a larger lattice had been used.

We start the presentation of the results by plotting, in Figs. 1 and 2, transverse widths  $\sigma_n$  versus the chemical potential for stationary unstaggered solitons of the on-site and inter-site types, respectively, found in both models 1 and 2 [recall that the vanishing field corresponds to  $\sigma_n = 1$ , see Eqs. (12) and (22)]. It is evident that these characteristics of the soliton families are close for both models, with some difference observed in central parts of the solitons.

To outline the entire existence region for the fundamental solitons, we followed the usual approach, identifying it as the region where CW (continuous-wave) solutions are modulationally unstable, hence the existence of bright solitons should be expected. The CW solutions can be easily found from stationary equations (25) and (26) in the form of

$$u_n = U e^{-i\mu t}, \quad \mu_{\text{CW}} = [1 + (3/2)gU^2] / \sqrt{1 + gU^2}, \quad \sigma_n^2 = 1 + gU^2, \quad (28)$$

which shows that in the case of the attractive interaction,  $g = -1$ , the amplitude of the CW solution is subject to constraint  $U < 1$ , and the respective chemical potential takes values  $\mu_{\text{CW}} < 1$ . Then, straightforward calculations yield a dispersion relation for frequency  $\Omega$  and wavenumber  $q$  of small modulational perturbations around the CW

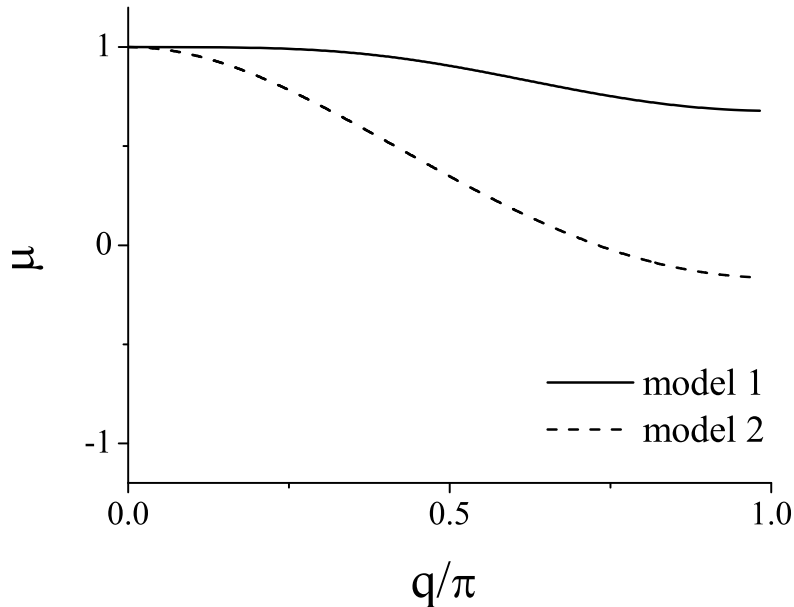


FIG. 3: The CW solutions are unstable to modulational perturbations in regions below curves  $\mu(q)$ , which are determined by condition  $\Omega^2 > 0$ , see Eq. (29). The solid and dashed curves correspond to models 1 and 2, respectively. The figure pertains to  $C = 0.8$ .

solution:

$$\Omega^2 = -2A \left[ 2A + \frac{2gU^2}{\sqrt{1+gU^2}} - \frac{g^2U^4}{2(1+gU^2)(\sqrt{1+gU^2}+D)} \right], \quad (29)$$

where  $A \equiv 2C \sin^2(q/2)$ , and  $D = A$  in model 2,  $D = 0$  in model 1. Analysis of this dispersion relation demonstrates that, in either model, the CW solution is unstable for  $\mu < 1$  against long-wave perturbations (for small values of  $q$ ), see Fig. (3).

In the case of the repulsive contact interactions,  $g > 0$ , one may expect the existence of *staggered* discrete solitons [15]. The analysis of the modulational instability of the respective staggered CW solutions (not given here in detail) shows that, for both models, the staggered CW states are indeed unstable in their entire existence region ( $\mu > 1$ ), which indicates that staggered solitons may exist at  $\mu > 1$  in either model. The further study of model 1 indicates that it supports strongly localized (tightly pinned) staggered solitons of the fundamental type (as reported before, see Figs. 20-23 in Ref. [16]). Model 2 reproduces only low-amplitude tightly pinned staggered modes near the lower boundary of the existence region. Those solutions are not displayed here, as the objective of the work is to focus on unstaggered solitons in the case of the self-attraction, when the difference of both models, 1 and 2, from the ordinary discrete cubic NLSE is most essential.

### B. The norm and free energy of fundamental unstaggered solitons

The power (norm) of unstaggered solitons in the two models,  $P = \sum_{n=1}^N |u_n|^2$ , and their free energy,  $G \equiv H - \mu P$ , where  $H$  is obtained by inserting stationary solution (24) into expressions (22) or (23), are compared in Figs. (4), (5) and (6) for two values of the intersite-coupling constant,  $C = 0.2$  and  $C = 0.8$ . These values, which were used in Figs. 1 and 5, actually correspond, severally, to limit cases of strongly discrete and quasi-continual systems. It is seen that the norms and free energies of the soliton families in both models feature similar behaviors: the same sign of the slope,  $dP/d\mu$ , for both the on-site and inter-site modes, the equality of the on-site and inter-site free energies in the region of a small power and small  $|\mu|$  (wide solitons with a small amplitude). Quantitative differences between the norm and free energy between the two models are larger for higher values of  $C$ , i.e., closer to the continuum limit.

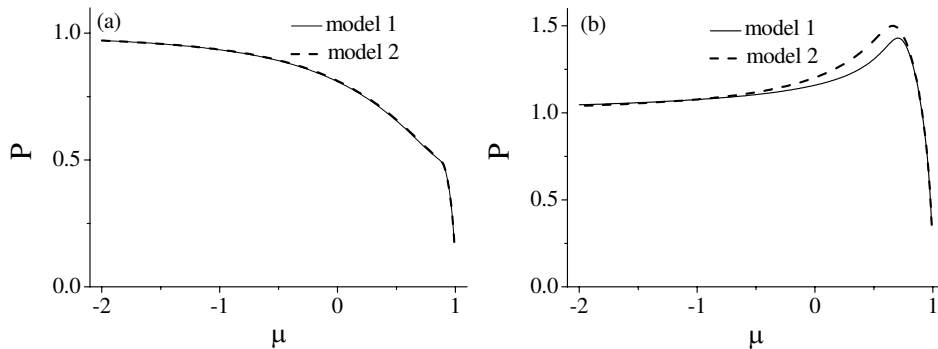


FIG. 4: The norm ("power")  $P$  versus chemical potential  $\mu$  for on-site fundamental solitons, in both models 1 and 2. The coupling constants are  $C = 0.2$  (a) and  $C = 0.8$  (b), which correspond to strongly discrete systems and quasi-continual systems, respectively.

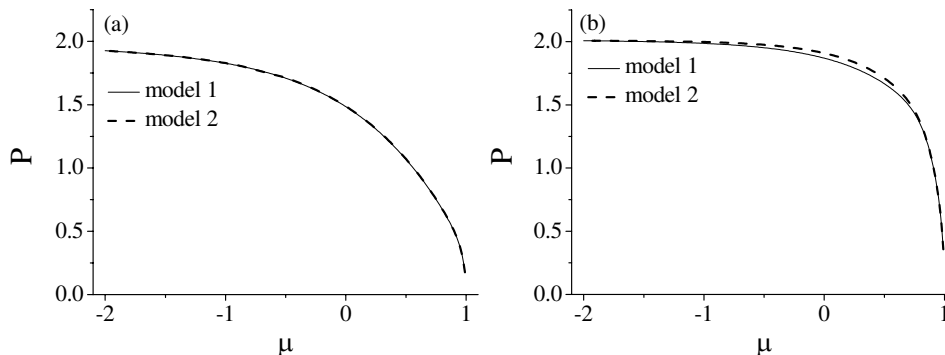


FIG. 5: The norm ("power")  $P$  versus chemical potential  $\mu$  for inter-site fundamental solitons, in models 1 and 2. The coupling constants are  $C = 0.2$  (a) and  $C = 0.8$  (b).

Some differences also appear in the region of large norms, which corresponds to very narrow solitons, where the  $P(\mu)$  curves show a trend to saturation. In particular, in that region amplitude  $u_n^2$  of the narrow solitons in models 2 may exceed 1, which is the absolute upper limit (collapse threshold) in model 1, as follows from Eq. (8). In fact, numerical results indicate at the existence of a similar limit in model 2, although it does not explicitly follow from Eqs. (21) and (22). Finding exact values for this limit is complicated by difficulties in obtaining accurate numerical results for very narrow (strongly pinned) solitons in model 2.

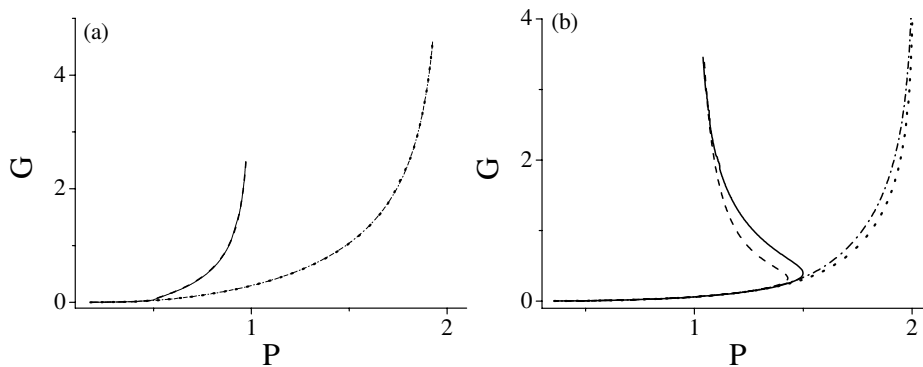


FIG. 6: Free energy  $G$  versus norm  $P$  for on-site and inter-site fundamental solitons, in both models 1 and 2, for  $C = 0.2$  (a) and  $C = 0.8$  (b). Solid and dashed lines correspond to the on-site solitons in models 2 and 1, respectively. Dotted and dashed-dotted lines represent, respectively, inter-site solitons in models 2 and 1.



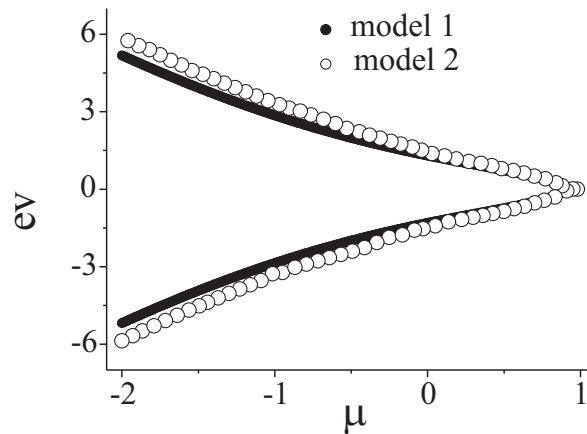


FIG. 7: Pure real unstable eigenvalues ("ev") for inter-site unstaggered solitons in models 1 and 2 are shown by black and white circles, respectively, for  $C = 0.2$ . Note that, in this case, pure real eigenvalues for on-site solitons have not been found.

### C. Dynamical considerations

The sufficient condition for soliton stability in the NPSE is the spectral condition according to which the corresponding eigenvalues, found from linearized equations for small perturbations, must not have a positive real part [14, 19]. Although the Vakhitov-Kolokolov (alias *slope*) stability criterion,  $dP/d\mu \leq 0$  [18], is not strictly applicable to the models with nonpolynomial nonlinearity we will also briefly comment it.

In Figs. (4) and (5),  $P(\mu)$  curves for the fundamental-soliton families have the same sign of the slope ( $dP/d\mu$ ) in models 1 and 2. Therefore, in the region of small  $P$  and small positive  $\mu$ , the on-site solitons may be stable in both models, according to the VK criterion. In all other cases, the on-site solitons are expected to be unstable. On the other hand, the VK criterion indicates the stability of inter-site solitons in the entire existence region, in both models.

To confirm the stability of the solitons, we have checked the spectral condition within the framework of the linear stability analysis, following the approach elaborated in Refs. [16, 17]). The results show that the fundamental unstaggered solitons in both models indeed have the same stability properties, as seen in Figs. (7) and (8). In particular, for on-site solitons the stability takes place only in a narrow region in the plane of  $(\mu, C)$ . This region is characterized by very close values of the norms of the on-site and inter-site solitons, hence a very small difference in the respective values the free energy, which, in turn, implies a very low Peierls-Nabarro barrier [16, 17], i.e., mobility of the solitons.

All conclusions concerning the mobility, perturbed evolution, and development of the collapse instability are qualitatively identical in both models. In particular, unstable inter-site modes which find on-site counterparts with close values of the norm (or free energy), and unstable on-site modes with close inter-site counterparts evolve into robust breathers, with almost no loss of the norm. In the opposite case, the instability leads to collapse of the localized modes. Our calculations show that collapse thresholds are nearly identical in models 1 and 2. In Ref. [16], it was found, in the framework of model 1, that (as mentioned above)  $u_n^2$  in soliton solutions cannot exceed 1; actually,  $u_n^2 = 1$  in Eq. (25) is the collapse threshold, which is determined by the singular structure of the on-site nonlinearity. A similar trend is demonstrated by numerical results obtained in model 2.

Summarizing this section, we conclude that both discrete models, 1 and 2, translate fundamental properties of bright solitons, known in the 1D continual NPSE, into the discrete setting in essentially the same way (for the discrete model of type 1, the correspondence with the continual equation was demonstrated in recent work [20]). The most significant among these properties is the possibility to describe the onset of the collapse in the framework of the 1D geometry.

## IV. CONCLUSION

The mean-field dynamics of BEC confined in a combination of a cigar-shaped trap and axial OL (optical-lattice) potential, is well approximated by the 1D NPSE (nonpolynomial Schrödinger equation), in both continual [4, 20] and discrete settings [16, 17]. In particular, both versions of the NPSE admit a possibility to describe the onset of the collapse of the localized modes in the framework of the 1D approximation, thus making this approximation compliant with the well-known fundamental property of the self-attractive BEC confined in tight traps. The objective of the

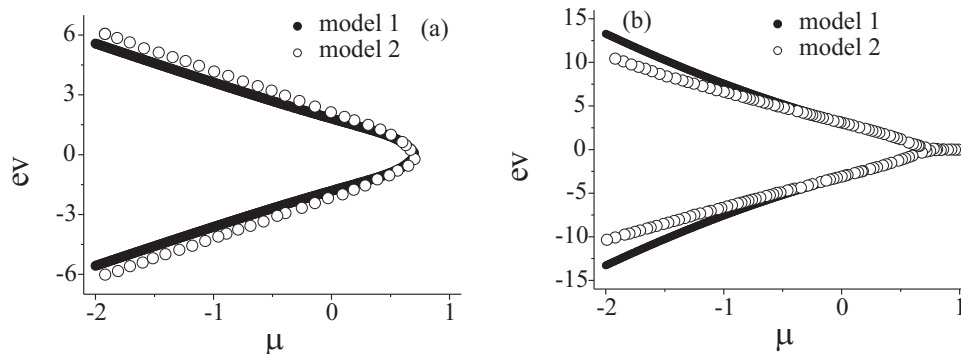


FIG. 8: The same as in Fig. 7, but at  $C = 0.8$ . In this case, plots (a) and (b) display the eigenvalues for the on-site solitons and inter-site solitons, respectively.

present work was to verify the relevance of the description based on the discrete limit of the NPSE-type equation, by comparing two alternative versions of this approximation: the previously derived one ("model 1"), which is based on the reduction of the underlying 3D GPE to 1D continual NPSE, followed by its discretization, and the new "model 2", whose derivation starts with the discretization of the 3D GPE, followed by the reduction of the dimension. The two steps of the derivation, *viz.*, the dimension reduction and discretization, are apparently non-commutative, and, accordingly, final forms of the two models appear to be vastly different; in particular, model 1 reduces to a single discrete equation for the wave function, while model 2 includes an additional equation for the transverse width. Nevertheless, the numerical solutions for families of fundamental unstaggered bight solitons produce *very similar* results in *both models*, as concerns their existence and stability, and, especially, the crucially important feature – the collapse threshold. A difference between the two models was found too, as model 2 (the newly introduced one) does not reproduce the region of high-amplitude strongly pinned narrow unstaggered and staggered modes, which was predicted in model 1. Actually, that feature of model 1 is impugnable, as it is not reproduced by the continual NPSE with the strong OL potential, as noted in Ref. [17]. In this respect, model 2 (the novel one), although having a more cumbersome mathematical form, seems physically preferable.

G.G., A.M. and Lj.H. acknowledge support from the Ministry of Science, Serbia (through project 141034). L.S. and B.A.M. appreciate a partial support from CARIPARO Foundation, through "Progetti di Eccellenza 2006". The work of B.A.M. was also supported, in a part, by the German-Israel Foundation through grant No. 149/2006.

- 
- [1] A. J. Leggett, *Quantum Liquids* (Oxford University Press, Oxford) (2006).
  - [2] V. M. Pérez-García, H. Michinel and H. Herrero, *Phys. Rev. A* **57**, 3837 (1998).
  - [3] A. E. Muryshev, G. V. Shlyapnikov, W. Ertmer, K. Sengstock and M. Lewenstein, *Phys. Rev. Lett.* **89**, 110401 (2002).
  - [4] L. Salasnich, *Laser Phys.* **12**, 198 (2002); L. Salasnich, A. Parola, and L. Reatto, *Phys. Rev. A* **65**, 043614 (2002); *ibid.* **70**, 013606 (2004); *ibid.* **72**, 025602 (2005); L. Salasnich and B. A. Malomed, *ibid.* **74**, 053610 (2006); L. Salasnich and B. A. Malomed and F. Toigo, *ibid.* **76**, 063614 (2007).
  - [5] L. Salasnich, arXiv:0907.1248v1 (2009).
  - [6] S. Sinha, A. Y. Cherny, D. Kovrizhin and J. Brand, *Phys. Rev. Lett.* **96**, 030406 (2006).
  - [7] L. Khaykovich and B. A. Malomed, *Phys. Rev. A* **74**, 023607 (2006).
  - [8] S. De Nicola, B. A. Malomed and R. Fedele, *Phys. Lett. A* **360**, 164 (2006); S. De Nicola, R. Fedele, D. Jovanovic, B. A. Malomed, M. A. Man'ko, V. I. Man'ko and P. K. Shukla, *Eur. Phys. J. B* **54**, 113 (2006).
  - [9] R. Carretero-González, D. J. Frantzeskakis and P. G. Kevrekidis, *Nonlinearity* **21**, R139–R202 (2008).
  - [10] K. E. Strecker, G. B. Partridge, A. G. Truscott and R. G. Hulet, *Nature* **417**, 150 (2002); see also K. E. Strecker, G. B. Partridge, A. G. Truscott, and R. G. Hulet, *New J. Phys.* **5**, 73 (2003).
  - [11] S. L. Cornish, S. T. Thompson and C. E. Wieman, *Phys. Rev. Lett.* **96**, 170401 (2006).
  - [12] L. Salasnich, A. Parola, L. Reatto, *Phys. Rev. A* **66**, 043603 (2002); L. Salasnich, *Phys. Rev. A* **70**, 053617 (2004); A. M. Mateo and V. Delgado, *Phys. Rev. Lett.* **97**, 180409 (2006); A. Muñoz Mateo and V. Delgado, *Phys. Rev. A* **77**, 013617 (2008).
  - [13] A. Trombettoni and A. Smerzi, *Phys. Rev. Lett.* **86**, 2353 (2001); F. Kh. Abdullaev, B. B. Baizakov, S. A. Darmanyan, V. V. Konotop, and M. Salerno, *Phys. Rev. A* **64**, 043606 (2001); G. L. Alfimov, P. G. Kevrekidis, V. V. Konotop, and M. Salerno, *Phys. Rev. E* **66**, 046608 (2002); R. Carretero-González, K. Promislow, *Phys. Rev. A* **66**, 033610 (2002); N. K. Efremidis and D. N. Christodoulides, *ibid.* **67**, 063608 (2003).
  - [14] G. Gligorić, A. Maluckov, Lj. Hadžievski, and B. A. Malomed, *Phys. Rev. A* **78** 063615 (2008).

- [15] M. A. Porter, R. Carretero-González, P. G. Kevrekidis, and B. A. Malomed, *Chaos* **15**, 015115 (2005).
- [16] A. Maluckov, Lj. Hadžievski, B. A. Malomed, and L. Salasnich, *Phys. Rev. A* **78**, 013616 (2008).
- [17] G. Gligorić, A. Maluckov, Lj. Hadžievski, B. A. Malomed, *Phys. Rev. A* **79**, 053609 (2009).
- [18] M. G. Vakhitov and A. A. Kolokolov, *Radiophys. Quantum Electron.* **16**, 783 (1973); L. Bergé, *Phys. Rep.* **303**, 259 (1998).
- [19] Y. Sivan, B. Ilan and G. Fibich, *Phys. Rev. E* **78**, 046602 (2008).
- [20] G. Gligorić, A. Maluckov, Lj. Hadžievski, B. A. Malomed, *J. Phys. B: At. Mol. Opt. Phys.* **42**, 145302 (2009).